



A mountain research station for clouds and turbulence

H. Siebert et al.

This discussion paper is/has been under review for the journal Atmospheric Measurement Techniques (AMT). Please refer to the corresponding final paper in AMT if available.

Schneefernerhaus as a mountain research station for clouds and turbulence – Part 2: Cloud microphysics and fine-scale turbulence

H. Siebert¹, R. A. Shaw², J. Ditas⁵, T. Schmeissner¹, S. P. Malinowski³, E. Bodenschatz⁴, and H. Xu⁴

¹Leibniz Institute for Tropospheric Research, Leipzig, Germany

²Department of Physics, Michigan Technological University, Michigan, USA

³University of Warsaw, Warsaw, Poland

⁴Max Planck Institute for Dynamics and Self-Organization (MPIDS), Göttingen, Germany

⁵Max Planck Institute for Chemistry, Mainz, Germany

Received: 16 December 2014 – Accepted: 18 December 2014 – Published: 15 January 2015

Correspondence to: H. Siebert (siebert@tropos.de)

Published by Copernicus Publications on behalf of the European Geosciences Union.

Title Page

Abstract

Introduction

Conclusions

References

Tables

Figures



Back

Close

Full Screen / Esc

Printer-friendly Version

Interactive Discussion



Abstract

Mountain research stations are advantageous not only for long-term sampling of cloud properties, but also for measurements that prohibitively difficult to perform on airborne platforms due to the true air speed or adverse factors such as weight and complexity of the equipment necessary. Some cloud-turbulence measurements, especially Lagrangian in nature, fall into this category. We report results from simultaneous, high-resolution and collocated measurements of cloud microphysical and turbulence properties during several warm cloud events at the Umweltforschungsstation Schneeföhnhaus (UFS) on Zugspitze in the German Alps. The data gathered was found to be representative of observations made with similar instrumentation in free clouds. The turbulence observed, shared all features known for high Reynolds number flows: it exhibited approximately Gaussian fluctuations for all three velocity components, a clearly defined inertial subrange following Kolmogorov scaling (power spectrum, and second and third order Eulerian structure functions), and highly intermittent velocity gradients, as well as approximately lognormal kinetic energy dissipation rates. The clouds were observed to have liquid water contents of order 1 g m^{-3} , and size distributions typical of continental clouds, sometimes exhibiting long positive tails indicative of large drop production through turbulent mixing or coalescence growth. Dimensionless parameters relevant to cloud-turbulence interactions, the Stokes number and settling parameter, are in the range typically observed in atmospheric clouds. Observed fluctuations in droplet number concentration and diameter suggest a preference for inhomogeneous mixing. Finally, enhanced variance in liquid water content fluctuations is observed at high frequencies, and the scale break occurs at a value consistent with the independently estimated phase relaxation time from microphysical measurements.

AMTD

8, 569–597, 2015

A mountain research station for clouds and turbulence

H. Siebert et al.

Title Page

Abstract

Introduction

Conclusions

References

Tables

Figures



Back

Close

Full Screen / Esc

Printer-friendly Version

Interactive Discussion



1 Introduction

Measurements of detailed interactions between turbulence and cloud processes are challenging. Airborne measurements allow for the most flexibility in going to the clouds of interest, but sample times are limited and measurements are inherently Eulerian in nature. We have investigated the suitability of making simultaneous and collocated cloud and turbulence measurements from a mountaintop research station, with the aim of characterizing the fine-scale turbulence and cloud microphysical properties. From a ground-based station it is possible to measure for extended periods of time and it also becomes feasible to perform measurements involving Lagrangian tracking of small volumes of cloudy air. The main question in this context is, in which ways the sampled clouds are influenced by the presence of the laboratory and the mountain, and whether the observed small-scale features are still representative of free atmospheric clouds.

The context of this study specifically addresses cloud-turbulence interactions. In a companion paper (Risius et al., 2015) the seasonal cloud and flow conditions and the large-scale turbulence structure are discussed. In this second part we consider the observed small-scale turbulence structure and cloud microphysical properties and compare them to conditions observed in free clouds with similar instrumentation. Specifically, we present high spatial resolution measurements of liquid water content, droplet diameter, and turbulent velocity and temperature fluctuations. The observations were performed at the Environmental Research Station (UFS) Schneefernerhaus in summer and fall 2009, and again in summer 2011. The measurements are analyzed and interpreted in a manner similar to data recorded in cumulus and stratocumulus clouds by the ACTOS platform Siebert et al. (2006a) in order to compare the two approaches.

More detail is given in Part 1 (Risius et al., 2015), but for completeness we briefly summarize relevant aspects of the measurement location here: The UFS is located in the German Alps near the top of Zugspitze (47°25′00″ N, 10°58′46″ E), the highest mountain in Germany (2962 ma.s.l.). The station is situated on the north side of the glacier and near the top of Zugspitze, at a height of about 2650 m. The UFS is a nine-

AMTD

8, 569–597, 2015

A mountain research station for clouds and turbulence

H. Siebert et al.

Title Page

Abstract

Introduction

Conclusions

References

Tables

Figures



Back

Close

Full Screen / Esc

Printer-friendly Version

Interactive Discussion



story building, constructed into the southern flank of the Zugspitze, and it experiences frequent immersion in clouds (cf., upper panel of Fig. 1). Due to the local topography, the winds measured at UFS are primarily in the east-west direction. The near uniformity of wind direction is a significant advantage for measurements because it allows instruments to be pointed in one fixed direction (e.g., see Fig. 1).

2 Experimental setup

Measurements of fine-scale turbulence and cloud microphysical properties in an Eulerian reference frame were performed from a fixed 3 m high mast with various measurement instruments (cf. Fig. 1). The mast was situated on the 9th-floor measurement platform during the first campaign (3–22 August 2009). The distance to the edge of this floor was about 2 m. The ultrasonic anemometers (hereafter called “sonics”) at the mast were orientated westward during both measurement periods.

The exact setup of the mast with the heights of the individual sensors is shown in Fig. 1. Two sonics of Solent HS type manufactured by Gill Ltd, Lymington, UK were mounted at heights of 1.80 and 2.55 m above the terrace. The measurement of the three-dimensional wind velocity vector and the virtual temperature are based on transit time measurements of ultrasonic pulses traveling between two transducers (for one velocity vector component) with and against the wind. The temporal resolution of the sonics is 100 Hz and the measuring resolution of the wind velocity and temperature are $\Delta u = 0.01 \text{ m s}^{-1}$ and $\Delta T = 0.01 \text{ K}$, respectively see Siebert and Muschinski (2001) for more details on the Solent HS). An ultra-fast thermometer (UFT) and a one-component hot-wire anemometer were fixed at a height of 2.20 m. The UFT is based on a $2.5 \mu\text{m}$ resistance wire protected against droplet impaction (cf. Haman et al., 1997) and the hot-wire anemometer uses a constant temperature approach (Comte-Bellot, 1976). Both instruments are sampled at a rate of 1 kHz.

Cloud microphysical variables were also measured from the mast. A particle volume monitor (PVM-100A, see Gerber, 1991) was positioned beside the UFT to measure the

A mountain research station for clouds and turbulence

H. Siebert et al.

Title Page

Abstract

Introduction

Conclusions

References

Tables

Figures



Back

Close

Full Screen / Esc

Printer-friendly Version

Interactive Discussion



A mountain research station for clouds and turbulence

H. Siebert et al.

[Title Page](#)[Abstract](#)[Introduction](#)[Conclusions](#)[References](#)[Tables](#)[Figures](#)[Back](#)[Close](#)[Full Screen / Esc](#)[Printer-friendly Version](#)[Interactive Discussion](#)

liquid water content (LWC) and the particle surface area (PSA). The intensity of laser light diffracted by a cloud droplet ensemble in a given measurement volume is related to the absolute volume concentration through use of a custom transmission filter in front of the detector. Liquid water contents are measurable within the full range of those observed in typical clouds (artifacts are known to be present for low concentrations of large droplets such as encountered in pristine environments, but this is not a problem for the microphysical conditions encountered at the UFS). Cloud droplet size distributions were measured with a phase-Doppler interferometer (PICT), located at a height of 1.50 m above ground. The measurement principle is based on heterodyne detection of Doppler-shifted light from individual droplets, resulting in a robust measurement of the droplet diameter and a single component of the droplet velocity vector (Chuang et al., 2008).

3 Data and analysis

The first part of this section presents a characterization of the turbulent flow under cloud-free conditions. This analysis complements that given in Part 1 (Risius et al., 2015): Part 1 focused on large-scale properties averaged over long times, and here we focus on high-resolution measurements with duration on the order of an hour. After characterizing the mean flow, we consider how closely the turbulence follows classical picture of homogeneous, isotropic turbulence at the fine scales by looking at velocity fluctuations, scaling for velocity power spectra and Eulerian structure functions, and velocity gradient and energy dissipation rate distributions. Here, the absence of cloud droplets allows hot-wire data to be used with full resolution (≈ 4 mm) because no despiking algorithm has to be applied to remove spikes in the data due to droplet impaction (Siebert et al., 2007). From this high-resolution data we address the question whether on the smallest observable scales the turbulence is similar to that observed in the free atmosphere, e.g., under conditions without the direct influence of the ground.

the conditions for the validity of Taylor's hypothesis (e.g., Willis and Deardorff, 1976). The linear trend for each of the six sub-records is included in Fig. 2 as solid orange line.

The velocity fluctuations $u'(t) = u(t) - \bar{u}$ were determined from a one-hour record divided into six 10 min-long sub-records, which were linearly de-trended to calculate the fluctuations $u'(t)$. For each sub-record, a matrix transformation was applied such that $\bar{v} = \bar{w} = 0$ and u was along the mean flow. In Fig. 3 the probability density functions (PDF) of the normalized velocity components u'_i/σ_{u_i} are presented. Each bin is an average over six sub-records. For reference, a Gaussian distribution is shown. The PDFs of all three velocity components can be well approximated by a Gaussian distribution, in agreement with observations for homogeneous and locally isotropic turbulence.

3.2 Hot-wire measurements: fine-scale turbulence

The fine scale turbulence was calculated from hot-wire data from clear air events. The one-dimensional data were sampled at $f_s = 1$ kHz, resulting in a mean spatial resolution of ≈ 4 mm. Only a short sub-record of the one-hour record of 600 s was considered for this analysis which is marked in Fig. 2 with a red box. The mean wind velocity of this sub-record is $\langle u \rangle = 4.2 \text{ ms}^{-1}$ with a SD of $\sigma_u = 1.4 \text{ ms}^{-1}$, which yields a turbulence intensity of $\sigma_u/\langle u \rangle \approx 0.33$, slightly below the critical value of 0.5 for the validity of Taylor's hypothesis (Willis and Deardorff, 1976).

In Fig. 4 the one-dimensional spectrum $f \cdot S_u(f)$ is plotted. The spectrum shows a clear inertial subrange scaling in the frequency range of 1 to 60 Hz (approximately 4 m to 7 cm). A linear fit was applied for that region (solid black line) yielding a slope of -0.64 , which is close to the theoretical value of $-2/3$. For frequencies below 1 Hz, the spectrum scatters due to statistical noise and for $f > 100$ Hz the spectrum drops off due to the increasing influence of dissipation. The turbulent energy dissipation rate per

A mountain research station for clouds and turbulence

H. Siebert et al.

Title Page

Abstract

Introduction

Conclusions

References

Tables

Figures



Back

Close

Full Screen / Esc

Printer-friendly Version

Interactive Discussion



unit mass ε can be estimated from the inertial range portion of the spectrum using

$$S(f) = \alpha \left(\frac{\bar{U}}{2\pi} \right)^{2/3} \varepsilon^{2/3} f^{-5/3}, \quad (1)$$

where α is a universal constant ($\alpha \approx 0.5$), and the factor $\bar{U}/2\pi$ is due to the conversion of the spectrum from wavenumber to frequency space. This approach leads to a mean of $\varepsilon = 8.5 \times 10^{-2} \text{ m}^2 \text{ s}^{-3}$, yielding a Kolmogorov length scale of $\eta = (\nu^3/\varepsilon)^{1/4} \approx 0.4 \text{ mm}$. This is still one order of magnitude below the resolution of our measurements but typical for highly turbulent parts of atmospheric clouds.

As an alternative method for estimating the mean energy dissipation rate, we consider the following relationships for n -th order structure functions of the longitudinal velocity vector component $D_{(n)} = \langle (u(x) - u(x+r))^n \rangle$:

$$D_{(2)}(r) = (C\varepsilon^{2/3})r^{2/3}, \quad (2)$$

where C has been found empirically to be approximately 2, and

$$D_{(3)}(r) = -\frac{4}{5}\varepsilon r. \quad (3)$$

Both functions are plotted in Fig. 5 together with their compensated form. The horizontal line marks the mean $\bar{\varepsilon} \approx 8.5 \times 10^{-2} \text{ m}^2 \text{ s}^{-3}$ as derived from the spectrum, which agrees within about 10% compared to the two estimates from the structure function relationships.

Small-scale turbulence at high Reynolds numbers is characterized by its intermittent nature, that is, periods of comparably small differences alternating with bursts of significantly increased gradients. This behavior can be better seen in the local velocity gradients du/dx . Here, $du = u_{i+1} - u_i$ and $dx = dt \cdot 1/2(u_i + u_{i+1})$, where $dt = 10^{-3} \text{ s}$ is the time resolution of the measurements. The normalized gradients

Title Page

Abstract

Introduction

Conclusions

References

Tables

Figures

◀

▶

◀

▶

Back

Close

Full Screen / Esc

Printer-friendly Version

Interactive Discussion



$\gamma = ((du/dx) - \overline{du/dx}) / \sigma_{du/dx}$ are shown in the upper panel of Fig. 6. Values up to 15 times the SDs are observed quite frequently, which is a typical feature of intermittency. The corresponding PDF in a semi-logarithmic plot (lower panel of Fig. 6) shows significantly enhanced tails compared to a Gaussian distribution, with the tails approximately exhibiting an exponential shape. Skewness $S = \overline{\gamma^3} = -0.4$ and kurtosis $K = \overline{\gamma^4} = 20$ were calculated. Wind-tunnel observations (Gylfason et al., 2004) suggest a power-law dependency of S and K on the Taylor microscale Reynolds number $Re_\lambda = \sigma_u^2 \sqrt{15}/(\epsilon\nu)$. For the observed $R_\lambda \approx 6200$ we obtain $S = -0.33 Re_\lambda^{0.09} \approx -0.7$ and $K = 0.91 Re_\lambda^{0.39} \approx 28$, which are in qualitative agreement with the directly calculated S and K . It has to be considered that the hot-wire measurements have a spatial resolution of about $10 \cdot \eta$ and the smallest relevant scales cannot be resolved, which can explain the underestimation of S and K . In free atmospheric clouds $K \approx 8$ has been observed at scales $\sim 20 \cdot \eta$ with strongly increasing values with increasing resolution (Siebert et al., 2010b).

Finally, we present the PDF of ϵ_τ derived from second-order structure functions (cf. Eq. 2). Here, each ϵ_τ is estimated from 100 ms-long sub-records; that is, the time series of ϵ_τ has a frequency of 10 Hz. Figure 7 shows the PDF of $\ln(\epsilon_\tau)$ together with a Gaussian fit in a semi-logarithmic plot. The good agreement of the measurements and the Gaussian distribution indicate that ϵ_τ is approximately lognormal, in accordance with the refined similarity theory of Kolmogorov (1962). Similar results have been found also for turbulent clouds (Siebert et al., 2010a, b) which supports the conclusion that on small scales the turbulence at UFS is representative of turbulence observed in “free” clouds, in spite of the possibility that on larger scales the turbulence differs in terms of isotropy and shear due to the influence of the orography.

A mountain research station for clouds and turbulence

H. Siebert et al.

Title Page

Abstract

Introduction

Conclusions

References

Tables

Figures



Back

Close

Full Screen / Esc

Printer-friendly Version

Interactive Discussion



3.3 Cloud microphysics and droplets in the turbulent velocity field

Here we present two examples of cloud microphysical properties representative of the variety of conditions typical at the UFS. On 11 August 2009 the UFS was exposed to relatively intermittent, thin clouds for several hours, of which a 40 min time period was selected. The data was recorded at 17:00 UTC. On 26 October 2009 the UFS was embedded in thick clouds for an extended period of time, and a 100 min time series of homogeneous coverage was selected which was recorded at around 08:00 UTC. On both days the flow was characterized by westerly directions. The temporal evolution of the cloud droplet size distribution is shown in Fig. 8. The 11 August period is dominated by extremely small cloud droplets, with intermittent bursts of droplets with diameter of approximately 8 to 12 μm , representative of microphysical conditions in small cumulus or thin stratocumulus clouds, either just in the process of formation, or during dissipation. The 26 October period shows a much more symmetric size distribution with a mean-diameter mode varying between 12 and 14 μm .

Time averaged probability density functions for the two periods are shown in Fig. 9. Estimation of the size distribution from the PICT requires normalization by the droplet-size-dependent detection cross section, which is obtained directly from the distribution of beam-transit times (Chuang et al., 2008). Specifically, the droplet number N_k in the k th size bin of width Δ is calculated following $N_k = (1/\Delta) \cdot (\tilde{N}_k/d_{\text{beam},k})/\sum_k(\tilde{N}_k/d_{\text{beam},k})$, where $d_{\text{beam},k}$ is the effective beam diameter for the k th size bin and \tilde{N}_k is the sampled number of droplets in the k th size bin. Immediately striking are the pronounced exponential large-droplet tails. It is apparent especially in the 26 October example that some mechanism for large droplet production is likely present, given the small but significant number of droplets with diameters above 25 μm . Given that peak liquid water contents for that date are only approaching $0.5\text{g},\text{m}^{-3}$, it is not obvious that coalescence is the source of large droplets: the large droplets are still too small to experience significant settling from higher levels in the cloud, but there are also indications that mixing and dilution have taken place, suggesting that the liquid

Title Page

Abstract

Introduction

Conclusions

References

Tables

Figures



Back

Close

Full Screen / Esc

Printer-friendly Version

Interactive Discussion



A mountain research station for clouds and turbulence

H. Siebert et al.

Title Page

Abstract

Introduction

Conclusions

References

Tables

Figures

◀

▶

◀

▶

Back

Close

Full Screen / Esc

Printer-friendly Version

Interactive Discussion



water content could have been higher earlier in the evolution of the cloud. We speculate, however, that mechanisms related to turbulent mixing may be important, including the production of large droplets within diluted cloud regions (Cooper et al., 2013) or through vertical cycling on time scales shorter than the phase relaxation time (Korolev et al., 2013). We will consider aspects of these two mechanisms later in this section, specifically, signatures of homogeneous vs. inhomogeneous mixing, and estimation of the phase relaxation time.

The microphysical conditions sampled in these two examples are quite representative of those measured in free clouds. We may also consider which part of the dimensionless parameter space they lie in with respect to droplet inertia and sedimentation effects relevant to particle-turbulence interactions (e.g., Siebert et al., 2010a). The importance of droplet inertia in response to a turbulent flow can be quantified by the Stokes number

$$St = \frac{\tau_d}{\tau_\eta} = \frac{\rho_w}{\rho_a} \frac{d^2}{18} \sqrt{\frac{\varepsilon}{\nu^3}} \propto d^2 \sqrt{\varepsilon}, \quad (4)$$

where $\tau_\eta = (\nu/\varepsilon)^{1/2}$ is the Kolmogorov time scale and $\tau_d = (\rho_w/\rho_a)(d^2/18\nu)$ is the inertial droplet response time. The relative importance of gravitational settling can be quantified through the ratio of terminal velocity $v_t = g\tau_d$ and Kolmogorov velocity $v_\eta = (\nu\varepsilon)^{1/4}$

$$Sv = \frac{\tau_d \cdot g}{v_\eta} = \frac{\rho_w}{\rho_a} \frac{d^2 g}{18 \varepsilon^{1/4} \nu^{5/4}} \propto \frac{d^2}{\varepsilon^{1/4}}. \quad (5)$$

Figure 10 shows a scatter plot of $\langle Sv|St \rangle$ points for both cloud samples, where each point represents an average over one second. The mean droplet diameter \bar{d} over the one-second period has been calculated by applying the appropriate sample-volume correction $\bar{d} = \sum_i (d_i/d_{\text{beam},i}) / \sum_i (1/d_{\text{beam},i})$. The turbulent energy local dissipation rate is obtained from the sonic data, using similar processing as described by Siebert et al. (2006b).

A mountain research station for clouds and turbulence

H. Siebert et al.

Title Page

Abstract

Introduction

Conclusions

References

Tables

Figures



Back

Close

Full Screen / Esc

Printer-friendly Version

Interactive Discussion



Although the energy dissipation rates are quite similar for both measurement periods (see middle panel of Fig. 9), the two scatter-plots significantly differ due to the contrasting microphysical conditions: both St and Sv have d^2 dependence, resulting in relatively high sensitivity to the distinct mean droplet diameters. However, both data show similar values as found by Siebert et al. (2010a) for free continental clouds (not shown here). For contrast, two examples of a maritime cloud situation with larger droplets, measured during the CARRIBA campaign, are also shown in Fig. 10. These cloud data were sampled in shallow trade wind cumuli under clean conditions, and the large droplet diameters yield significantly higher St and Sv . This allows us to conclude that, from the perspective of fine-scale droplet-turbulence interactions, cloud droplets in a turbulent flow at the UFS are representative of free atmospheric clouds in a continental environment.

We now consider two further ways in which the turbulence can interact with cloud microphysics. First, turbulence leads to mixing between the cloud and clear-air environment, with corresponding reduction in liquid water content. That reduction, however, can take place as a reduction in either the droplet number density n or the mean droplet diameter d , and the details of how it occurs give some hints as to the type of mixing that is occurring (e.g., Jensen et al., 1985). For homogeneous mixing, both n and d are reduced monotonically, as for a population of droplets exposed to identical (well mixed) thermodynamic conditions. For inhomogeneous mixing, some subset of the droplets is exposed to sub-saturated conditions and evaporates completely, while the majority of the droplets experience no evaporation. The result is a reduction in n but little or no reduction in d . The homogeneous limit can be calculated if the environmental humidity is known, but in this case it is not, so we plot d vs. n and consider qualitatively whether the measured number densities and droplet sizes (for equal-time bins) tend to prefer one monotonic decrease of n and d , or decrease of n without d . We show data from the long time record taken on 26 October in Fig. 11. Both n and d are obtained from the PICT measurements of the droplet size distribution, and each point in the figure corresponds to a 2 s average (approximately 8 m length). The data show wide variation in

n with an almost uniform value of d , clearly suggesting prevalence of inhomogeneous mixing.

The second question is concerning the range of time scales for turbulent eddies within the inertial subrange, relative to the cloud supersaturation, or phase relaxation time. Specifically, it has been suggested by Mazin (1999), with empirical support from Davis et al. (1999) and Gerber et al. (2001), that the smallest, high-frequency eddies should experience larger variance in microphysical properties. This follows the qualitative argument that for eddy time scales of the same order as or less than the phase relaxation time, the supersaturation is not able to reach its quasi-steady value for a given vertical velocity. Therefore, droplets will grow in an environment different than that typically assumed in steady-state models. It has been suggested that this can lead to broadening of the droplet size distribution (Korolev et al., 2013).

We have selected two subsets of the 11 August and 26 October data sets (cf., Fig. 9), for calculation of power spectral density of liquid water content. Special care was taken to ensure a steady mean wind direction from west to minimize possible bias of the liquid water statistics from air not entering the PVM directly through its opening. The length of the time series were 130 s for 11 August and 65 s for 26 October, and the LWC data were processed at the full sampling frequency of 1 kHz. The power spectra are shown in Fig. 12, and the flattening of the spectra at high frequencies is clearly evident. Following the argument of Mazin (1999), we estimate the transition frequency for this flattening and use the mean flow speed and Taylor's hypothesis to convert the frequency to an eddy length scale. This length scale can be compared to an eddy length scale estimated from the phase relaxation time, which is independently calculated from direct measurement of the droplet size distribution with the phase Doppler interferometer. Using the measured turbulent kinetic energy dissipation rate and Kolmogorov scaling for the inertial subrange, this time scale is converted to an eddy length scale for phase relaxation.

The liquid water content power spectra in Fig. 12 show approximate transitions at frequencies of 2 to 3 Hz for both dates. The mean flow speeds during the sub-records

A mountain research station for clouds and turbulence

H. Siebert et al.

Title Page

Abstract

Introduction

Conclusions

References

Tables

Figures



Back

Close

Full Screen / Esc

Printer-friendly Version

Interactive Discussion



A mountain research station for clouds and turbulence

H. Siebert et al.

Title Page

Abstract

Introduction

Conclusions

References

Tables

Figures



Back

Close

Full Screen / Esc

Printer-friendly Version

Interactive Discussion



spatial scales of relevance to cloud microphysical processes. Time series of droplet number density, liquid water content, and local velocity gradients and energy dissipation rate, as well as averaged cloud droplet size distributions, are very comparable with measurements of boundary-layer-topped cloud properties from prior ACTOS (Airborne Cloud Turbulence Observation System) field projects under continental conditions. Comparisons of relevant dimensionless parameters for droplet inertial effects, the Stokes number and the settling parameter, show similar ranges as in “free” clouds, suggesting that the mountain top station is a reasonable location for making measurements of cloud-turbulence interactions.

This work was motivated primarily by the desire to make cloud-turbulence measurements that would be difficult to obtain from an airborne system. Specifically, techniques for Lagrangian tracking of particles in turbulent flows have provided new perspectives on the behavior of inertial particles in turbulence (Ayyalasomayajula et al., 2006; Gibert et al., 2012; Bewley et al., 2013). The measurements presented in these two companion papers support the argument that the UFS Schneefernerhaus is a suitable location for detailed Lagrangian measurements of cloud droplets in turbulence, both of which have properties representative of free clouds.

Acknowledgements. We thank Thomas Conrath for help with logistical aspects of the experiment and to Matthew Beals and Amanda Shaw for help with data processing. We are grateful to Markus Neumann and the staff at UFS for their technical help at UFS and the Bavarian Umweltministerium for the financial support of the station. Financial support from Max Planck Society, Deutsche Forschungsgemeinschaft (DFG) through the SPP 1276 Metström, the EU COST Action MP0806 “Particles in Turbulence,” and through the US National Science Foundation (NSF grant AGS-1026123) are gratefully acknowledged.

References

Ayyalasomayajula, S., Gylfason, A., Collins, L. R., Bodenschatz, E., and Warhaft, Z.: Lagrangian measurements of inertial particle accelerations in grid generated wind tunnel turbulence, *Phys. Rev. Lett.*, 97, 144507, doi:10.1103/PhysRevLett.97.144507, 2006. 583

A mountain research station for clouds and turbulence

H. Siebert et al.

Title Page

Abstract

Introduction

Conclusions

References

Tables

Figures



Back

Close

Full Screen / Esc

Printer-friendly Version

Interactive Discussion



- Bewley, G. P., Saw, E.-W., and Bodenschatz, E.: Observation of the sling effect, *New J. Phys.*, 15, 083051, doi:10.1088/1367-2630/15/8/083051, 2013. 583
- Chuang, P. Y., Saw, E. W., Small, J. D., Shaw, R. A., Sipperley, C. M., Payne, G. A., and Bachalo, W.: Airborne phase doppler interferometry for cloud microphysical measurements, *Aerosol Sci. Technol.*, 42, 685–703, 2008. 573, 578
- Comte-Bellot, G.: Hot-wire anemometry, *Annu. Rev. Fluid Mech.*, 8, 209–231, 1976. 572
- Cooper, W. A., Lasher-Trapp, S. G., and Blyth, A. M.: The influence of entrainment and mixing on the initial formation of rain in a warm cumulus cloud, *J. Atmos. Sci.*, 70, 1727–1743, 2013. 579
- Davis, A. B., Marshak, A., Gerber, H., and Wiscombe, W. J.: Horizontal structure of marine boundary layer clouds from centimeter to kilometer scales, *J. Geophys. Res.*, 104, 6123–6144, 1999. 581
- Gerber, H.: Direct measurement of suspended particulate volume concentration and far-infrared extinction coefficient with a laser-diffraction instrument, *Appl. Optics*, 30, 4824–4831, 1991. 572
- Gerber, H., Jensen, J. B., Davis, A. B., Marshak, A., and Wiscombe, W. J.: Spectral density of cloud liquid water content at high frequencies, *J. Atmos. Sci.*, 58, 497–503, 2001. 581, 582
- Gibert, M., Xu, H., and Bodenschatz, E.: Where do small, weakly inertial particles go in a turbulent flow?, *J. Fluid Mech.*, 698, 160–167, 2012. 583
- Gylfason, A., Ayyalasomayajula, S., and Warhaft, Z.: Intermittency, pressure and acceleration statistics from hot-wire measurements in wind-tunnel turbulence, *J. Fluid Mech.*, 501, 213–229, 2004. 577
- Haman, K. E., Makulski, A., Malinowski, S. P., and Busen, R.: A new ultrafast thermometer for airborne measurements in clouds, *J. Atmos. Ocean. Tech.*, 14, 217–227, 1997. 572
- Jensen, J. B., Austin, P. H., Baker, M. B., and Blyth, A. M.: Turbulent mixing, spectral evolution and dynamics in a warm cumulus cloud, *J. Atmos. Sci.*, 42, 173–192, 1985. 580
- Kolmogorov, A. N.: A refinement of previous hypotheses concerning the local structure of turbulence in a viscous incompressible fluid at high Reynolds number, *J. Fluid Mech.*, 13, 82–85, 1962. 577
- Korolev, A., Pinsky, M., and Khain, A.: A new mechanism of droplet size distribution broadening during diffusional growth, *J. Atmos. Sci.*, 70, 2051–2071, 2013. 579, 581
- Mazin, I.: The effect of condensation and evaporation on turbulence in clouds, *Atmos. Res.*, 51, 171–174, 1999. 581, 582

A mountain research station for clouds and turbulence

H. Siebert et al.

Title Page

Abstract

Introduction

Conclusions

References

Tables

Figures



Back

Close

Full Screen / Esc

Printer-friendly Version

Interactive Discussion



- Risius, S., Xu, H., Di Lorenzo, F., Xi, H., Siebert, H., Shaw, R. A., and Bodenschatz, E.: Schneefernerhaus as a mountain research station for clouds and turbulence – Part 1: Flow conditions and large-scale turbulence, *Atmos. Meas. Tech. Discuss.*, 8, 541–568, doi:10.5194/amtd-8-541-2015, 2015. 571, 573
- 5 Siebert, H. and Muschinski, A.: Relevance of a tuning-fork effect for temperature measurements with the Gill Solent HS Ultrasonic Anemometer-Thermometer, *J. Atmos. Ocean. Tech.*, 18, 1367–1376, 2001. 572
- Siebert, H., Wendisch, M., Conrath, T., Teichmann, U., and Heintzenberg, J.: A new tethered balloon-borne payload for fine-scale observations in the cloudy boundary layer, *Bound.-Lay Meteorol.*, 106, 461–482, 2003. 582
- 10 Siebert, H., Franke, H., Lehmann, K., Maser, R., Saw, E. W., Schell, D., Shaw, R. A., and Wendisch, M.: Probing fine-scale dynamics and microphysics of clouds with helicopter-borne measurements, *B. Am. Meteorol. Soc.*, 87, 1727–1738, 2006a. 571
- Siebert, H., Lehmann, K., and Wendisch, M.: Observations of small scale turbulence and energy dissipation rates in the cloudy boundary layer, *J. Atmos. Sci.*, 63, 1451–1466, 2006b. 579
- 15 Siebert, H., Lehmann, K., and Shaw, R.: On the use of a hot-wire anemometer for turbulence measurements in clouds, *J. Atmos. Ocean. Tech.*, 24, 980–993, 2007. 573
- Siebert, H., Gerashchenko, S., Lehmann, K., Gylfason, A., Collins, L. R., Shaw, R. A., and Warhaft, Z.: Towards understanding the role of turbulence on droplets in clouds: in situ and laboratory measurements, and numerical modeling, *Atmos. Res.*, 97, 426–437, 2010a. 574, 577, 579, 580, 595
- 20 Siebert, H., Shaw, R. A., and Warhaft, Z.: Statistics of small-scale velocity fluctuations and internal intermittency in marine stratocumulus clouds, *J. Atmos. Sci.*, 67, 262–273, 2010b. 577
- 25 Siebert, H., Beals, M., Bethke, J., Bierwirth, E., Conrath, T., Dieckmann, K., Ditas, F., Ehrlich, A., Farrell, D., Hartmann, S., Izaguirre, M. A., Katzwinkel, J., Nuijens, L., Roberts, G., Schäfer, M., Shaw, R. A., Schmeissner, T., Serikov, I., Stevens, B., Stratmann, F., Wehner, B., Wendisch, M., Werner, F., and Wex, H.: The fine-scale structure of the trade wind cumuli over Barbados – an introduction to the CARRIBA project, *Atmos. Chem. Phys.*, 13, 10061–10077, doi:10.5194/acp-13-10061-2013, 2013. 595
- 30 Willis, G. E. and Deardorff, J. W.: On the use of Taylor's translation hypothesis for diffusion in the mixed layer, *Q. J. Roy. Meteor. Soc.*, 102, 817–822, 1976. 575

A mountain research station for clouds and turbulence

H. Siebert et al.

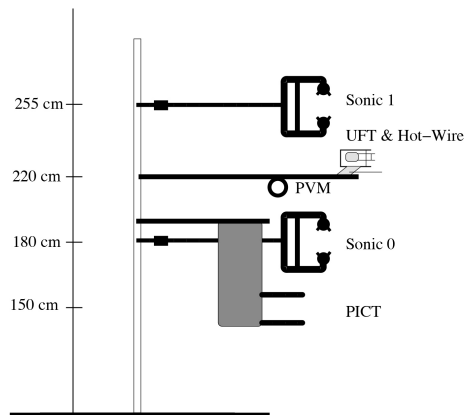


Figure 1. The picture shows the UFS partly immersed in cloud. The location of the experimental setup on 9th-floor is indicated by the yellow arrow. A schematic of the mast equipped with two sonics, ultra-fast thermometer (UFT), one-component hot-wire anemometer, particle volume monitor (PVM) for liquid water content measurements, and a phase-Doppler interferometer (PICT) is shown in the lower panel including the individual measurement heights above the terrace.

[Title Page](#)
[Abstract](#)
[Introduction](#)
[Conclusions](#)
[References](#)
[Tables](#)
[Figures](#)
[Back](#)
[Close](#)
[Full Screen / Esc](#)
[Printer-friendly Version](#)
[Interactive Discussion](#)


A mountain research station for clouds and turbulence

H. Siebert et al.

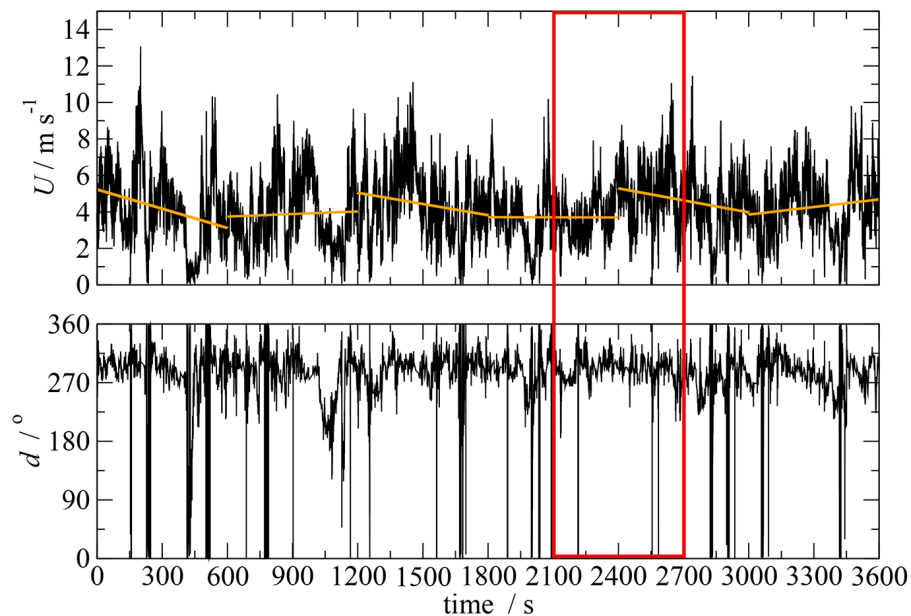


Figure 2. Time series of horizontal wind velocity $U = \sqrt{u^2 + v^2}$ and wind direction d . The solid orange lines mark the linear trend for each of the six 10 min-long sub-records. Data were measured with the upper sonic (S1) about 2.55 m above the surface.

[Title Page](#)[Abstract](#)[Introduction](#)[Conclusions](#)[References](#)[Tables](#)[Figures](#)[◀](#)[▶](#)[◀](#)[▶](#)[Back](#)[Close](#)[Full Screen / Esc](#)[Printer-friendly Version](#)[Interactive Discussion](#)

A mountain research station for clouds and turbulence

H. Siebert et al.

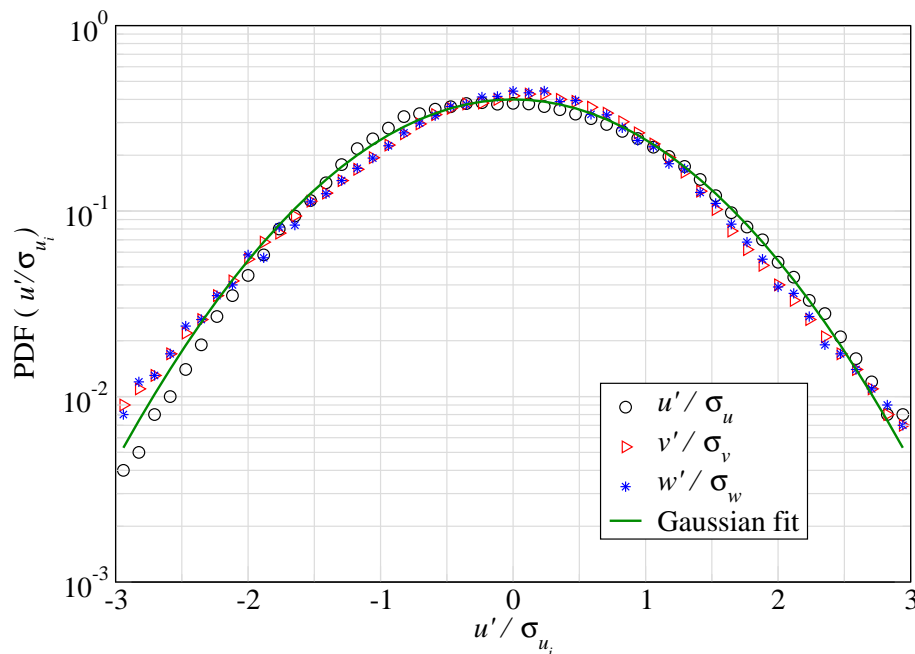


Figure 3. Probability density functions of normalized velocity component fluctuations u'_i/σ_{u_i} for the upper sonic. Each bin is the result of an average over six 10 min-long sub-records. The data is the same as for Fig. 2. The fluctuations are calculated from the linear de-trended sub-records. A Gaussian fit is given as reference.

[Title Page](#)[Abstract](#)[Introduction](#)[Conclusions](#)[References](#)[Tables](#)[Figures](#)[Back](#)[Close](#)[Full Screen / Esc](#)[Printer-friendly Version](#)[Interactive Discussion](#)

A mountain research station for clouds and turbulence

H. Siebert et al.

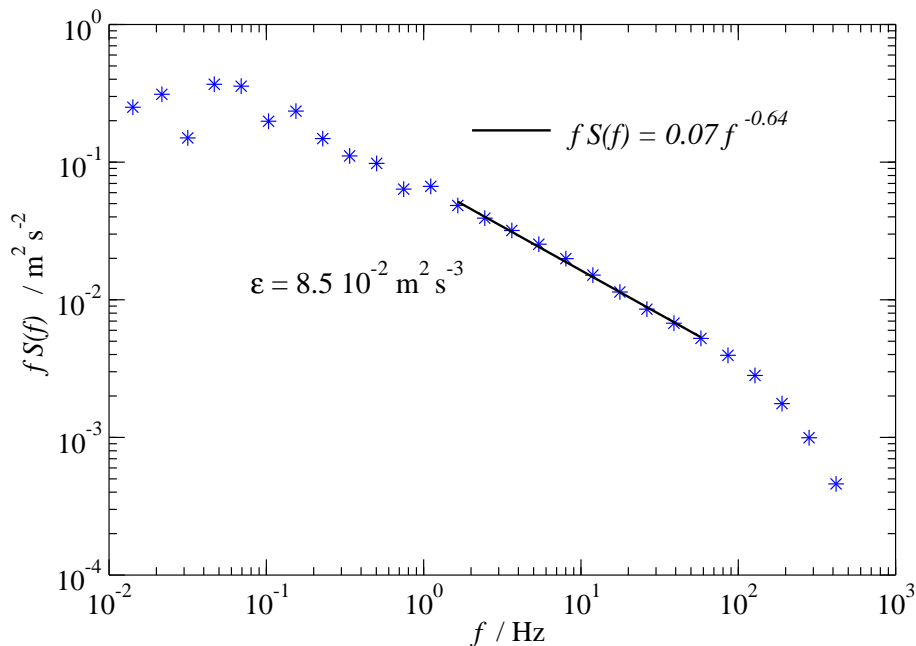


Figure 4. Power spectral density function $S(f)$ multiplied with frequency f as derived from a ten-minute sub-record (as indicated with in red in Fig. 2) of a one-component hot-wire. From an inertial sub-range fit (see black solid line), a mean energy dissipation rate of $\bar{\varepsilon} \approx 8.5 \times 10^{-2} \text{ m}^2 \text{ s}^{-3}$ was estimated.

Title Page

Abstract

Introduction

Conclusions

References

Tables

Figures

◀

▶

◀

▶

Back

Close

Full Screen / Esc

Printer-friendly Version

Interactive Discussion



A mountain research station for clouds and turbulence

H. Siebert et al.

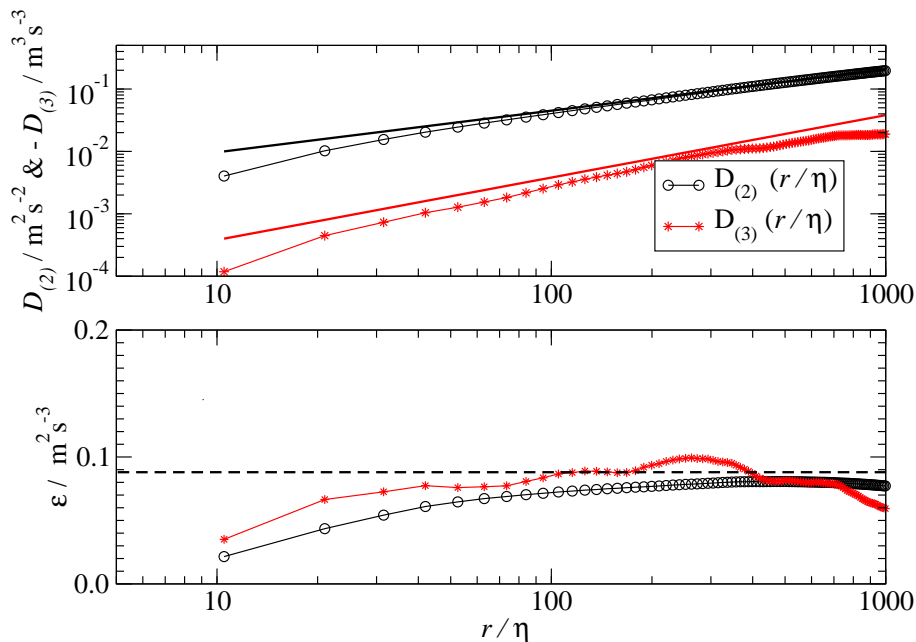


Figure 5. 2nd- and 3rd-order structure functions derived from hot-wire measurements with 1 ms time resolution (upper panel) and compensated structure functions yielding the energy dissipation rate ϵ as a function of r/η .

Title Page

Abstract Introduction

Conclusions References

Tables Figures

◀ ▶

◀ ▶

Back Close

Full Screen / Esc

Printer-friendly Version

Interactive Discussion



A mountain research station for clouds and turbulence

H. Siebert et al.

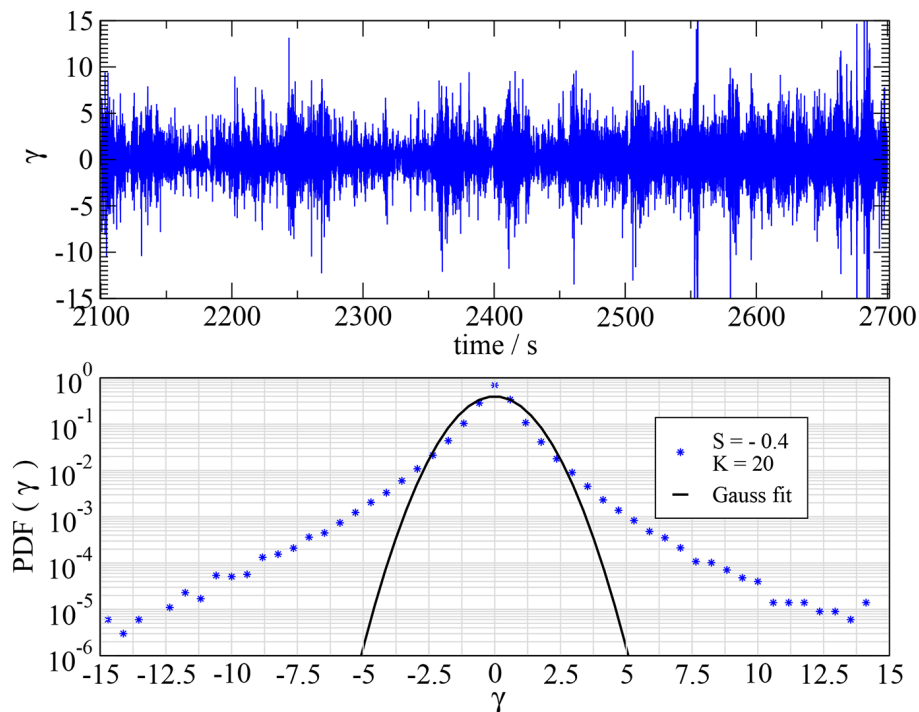


Figure 6. Upper panel: Ten-minute sub-record of normalized velocity gradients $\gamma = ((du/dx) - du/dx)/\sigma_{du/dx}$. The lower panel shows the corresponding PDF in semi-logarithmic plot with a Gaussian distribution for reference. The skewness $S = -0.4$ and the kurtosis $K = 20$.

Title Page

Abstract

Introduction

Conclusions

References

Tables

Figures



Back

Close

Full Screen / Esc

Printer-friendly Version

Interactive Discussion



A mountain research station for clouds and turbulence

H. Siebert et al.

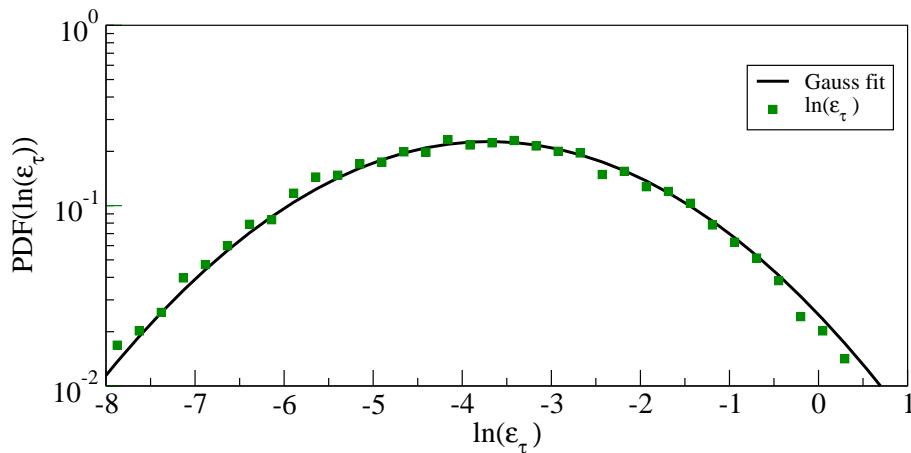


Figure 7. Probability density function (PDF) of $\ln(\epsilon_\tau)$ with $\tau = 0.1$ s estimated from a 10 min subrecord. A Gaussian distribution is plotted as reference.

[Title Page](#)[Abstract](#)[Introduction](#)[Conclusions](#)[References](#)[Tables](#)[Figures](#)[◀](#)[▶](#)[◀](#)[▶](#)[Back](#)[Close](#)[Full Screen / Esc](#)[Printer-friendly Version](#)[Interactive Discussion](#)

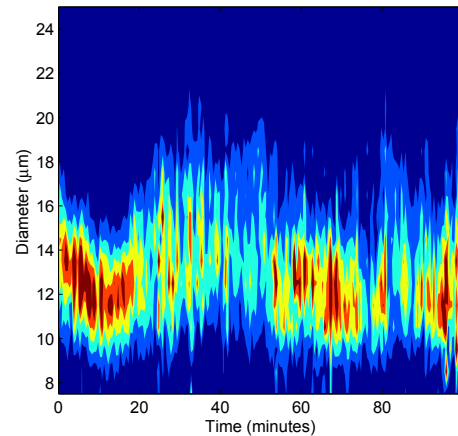
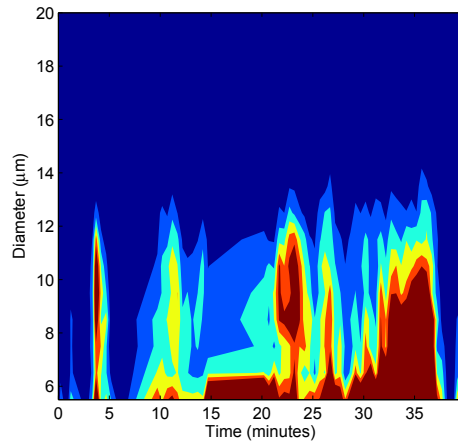


Figure 8. Temporal evolution of the cloud droplet size distribution during a 40 min time period on 11 August 2009 (top) and a 100 min period on 26 October 2009 (bottom). The color scheme corresponds to droplet number density. The size distributions were measured by the phase-Doppler interferometer (PICT).

A mountain research station for clouds and turbulence

H. Siebert et al.

Title Page

Abstract

Introduction

Conclusions

References

Tables

Figures

◀

▶

◀

▶

Back

Close

Full Screen / Esc

Printer-friendly Version

Interactive Discussion



A mountain research station for clouds and turbulence

H. Siebert et al.

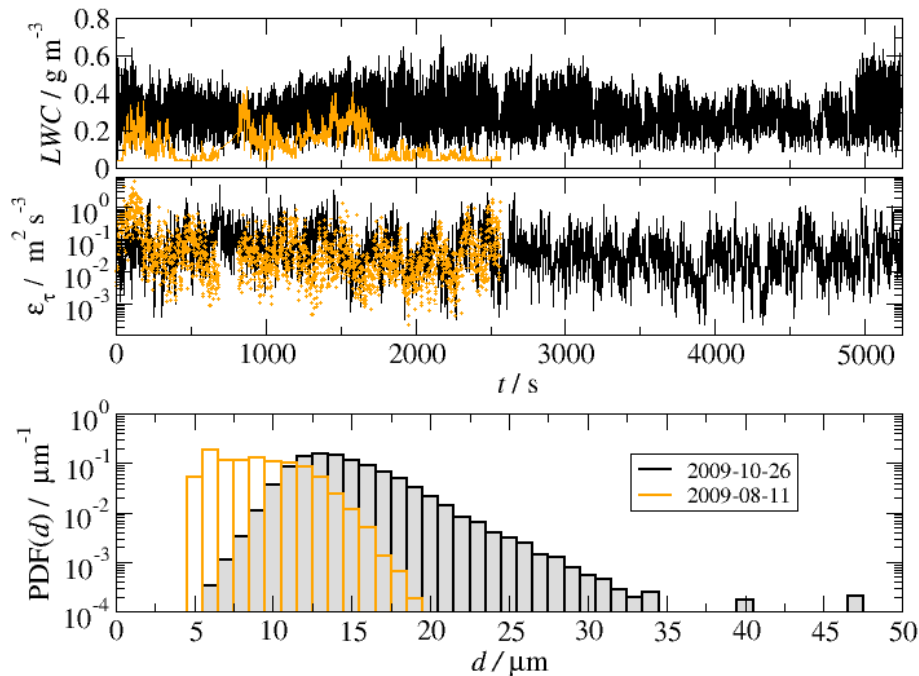


Figure 9. Time series of liquid water content LWC (top panel), local energy dissipation rate ϵ (middle panel), and probability density function for the droplet diameter PDF(d) (lower panel) as observed during the 100 min-long cloud period on 26 October 2009 (black lines) and the 40 min-long record on 11 August 2009 (orange lines).

A mountain research station for clouds and turbulence

H. Siebert et al.

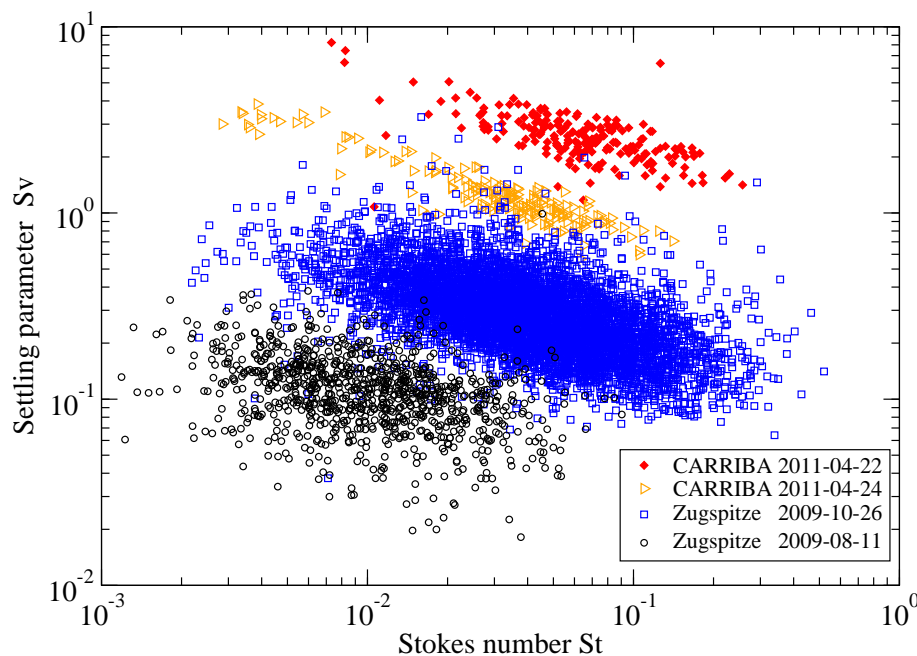


Figure 10. Dimensionless Stokes and settling parameter space. Each $(St|Sv)$ -point is based on a one-second average of cloud data. The CARRIBA data represents typical conditions for clean (red) and slightly more polluted (yellow) cases and provide a reference for typical trade wind cumuli (see Siebert et al., 2013, for more details). Data from small cumulus and stratocumulus clouds under continental conditions are not shown, but are nearly coincident with the Zugspitze values (Siebert et al., 2010a).

Title Page

Abstract

Introduction

Conclusions

References

Tables

Figures



Back

Close

Full Screen / Esc

Printer-friendly Version

Interactive Discussion



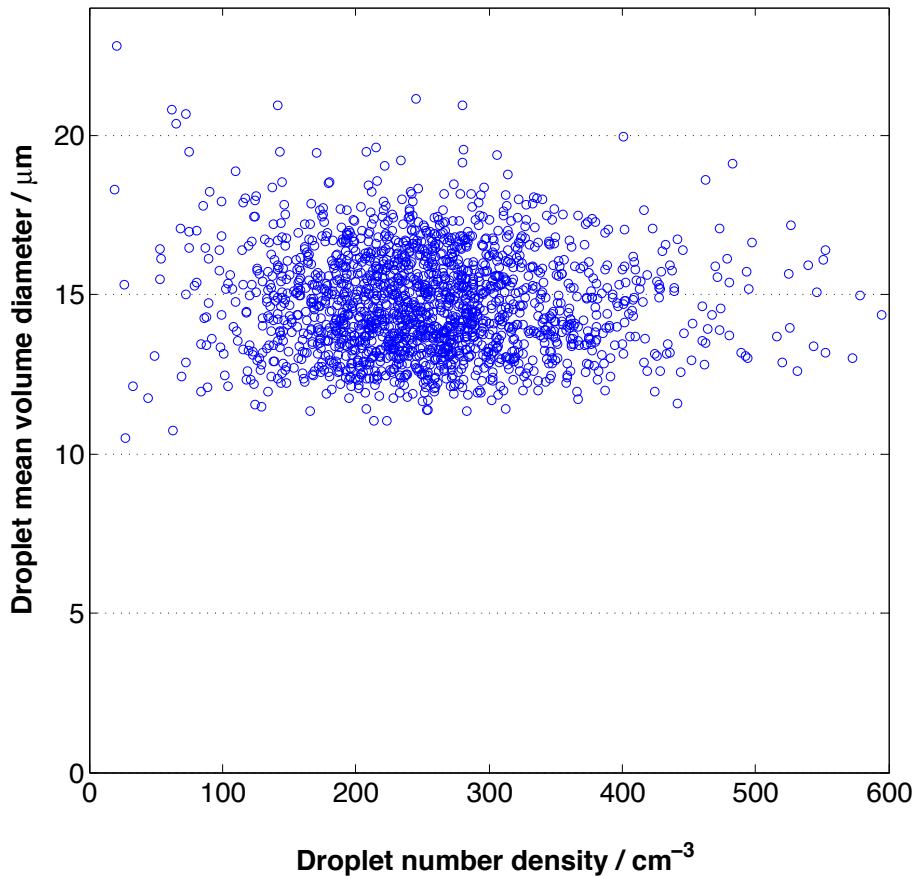


Figure 11. Mean-volume droplet diameter vs. droplet number density for 2 s intervals in the 26 October 2009 data set. The nearly horizontal distribution of points is indicative of inhomogeneous mixing.

A mountain research station for clouds and turbulence

H. Siebert et al.

Title Page	
Abstract	Introduction
Conclusions	References
Tables	Figures
◀	▶
◀	▶
Back	Close
Full Screen / Esc	
Printer-friendly Version	
Interactive Discussion	



A mountain research station for clouds and turbulence

H. Siebert et al.

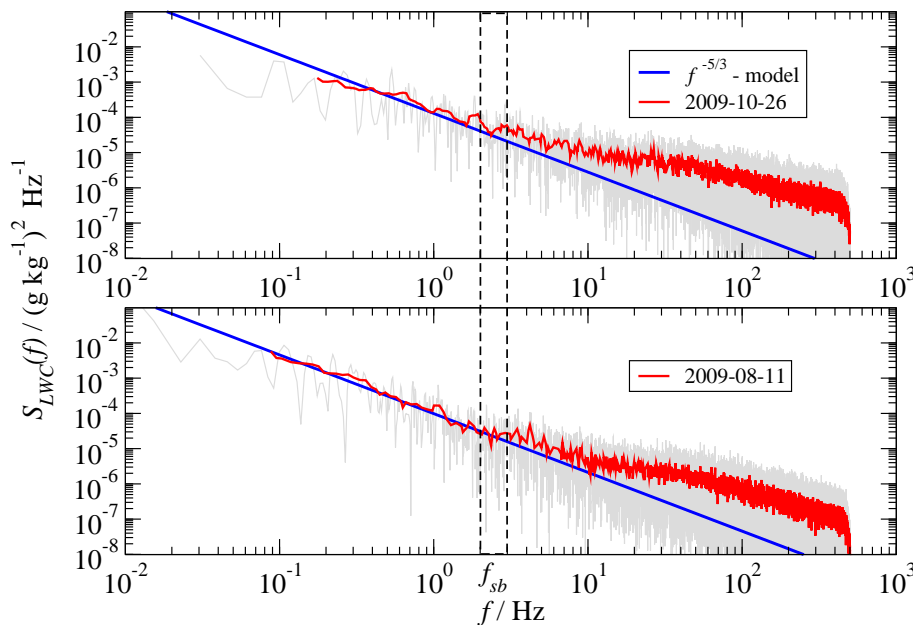


Figure 12. Power spectral densities of LWC for the 100 min-long cloud period on 26 October 2009 (upper panel) and the 40 min-long record on 11 August 2009 (lower panel). The solid blue line represents a $-5/3$ slope for inertial subrange scaling. The vertical line denotes the scale that corresponds to the phase relaxation time estimated from the phase Doppler measurements.

[Title Page](#)
[Abstract](#)
[Introduction](#)
[Conclusions](#)
[References](#)
[Tables](#)
[Figures](#)
[◀](#)
[▶](#)
[◀](#)
[▶](#)
[Back](#)
[Close](#)
[Full Screen / Esc](#)
[Printer-friendly Version](#)
[Interactive Discussion](#)
